Applied Numerical Modeling in Geomechanics – 2020 – Billaux, Hazzard, Nelson & Schöpfer (eds.) Paper: 02-02

DEM analysis of intact rock strength under confined tension

Haiying Huang[1] & Yifei Ma[2]
[1] *School of Civil and Environmental Engineering, Georgia Institute of Technology, Atlanta, GA, USA*
[2] *Department of Civil and Architectural Engineering, Lawrence Technological University, Southfield, MI, USA*

1 INTRODUCTION

When modeling behaviors of intact rock subjected to confined tension using continuum mechanics based methods, we generally take an approach by either extending a smooth failure envelope from triaxial compression, e.g. the Hoek-Brown criterion (Hoek & Martin 2014), or incorporating a tension cut-off, e.g. a Mohr-Coulomb criterion with a tension cut-off. With its root in the local tensile stress criterion, a tension cut-off is also included in the original Griffith's criterion and its generalization by Fairhurst (1964), intended specifically for the confined tension state. Essentially, we are making implicit assumptions about the underlying physics that while brittle fracture due to uniaxial tension and ductile shear failure due to triaxial compression are two end members of rock failure behaviors, there are different ways for the transition between the two members to occur.

Experimental research on rock behaviors under confined tension has been scarce. The seminal work by Brace (1964) is the primary source that provided experimental support for using a tension cut-off. Out of twenty triaxial extension tests conducted with dog-bone shaped specimens of five rock types, i.e., granite, quartzite, diabase and two dolomites, seven samples fail at axial stresses close to their uniaxial tensile strengths and with the failure planes more or less normal to the axial direction. The experimental work by Ramsey & Chester (2004) with Carrara marble seems to affirm the legitimacy of a tension cut-off and the existence of hybrid fracture as a transition from extension to shear failure. Combining evidences from fracture orientation, fracture surface morphology with stress state at failure, they showed that extension fracture is associated with signatures such as relatively constant peak tensile stress and near zero fracture angle, i.e., the angle between the normal of the fracture surface and the axial direction. For hybrid fracture, the fracture angle increases with the confining stress, while the peak axial stress decreases, but remains tensile. Shear fracture occurs when the peak axial stress becomes compressive.

In this work, we attempt to analyze the failure behaviors under confined tension through the perspectives of the distinct element method (DEM) with bonded spherical particles (e.g., Potyondy & Cundall 2004). Our prior development of a displacement-softening contact model (Ma & Huang 2018), which is modified from the parallel bond model in *PFC 5* (Itasca 2014a, b), can overcome the long-standing issue of low compressive over tensile strength ratio (UCS/UTS) in DEM modeling (Huang 1999). By decreasing the softening coefficient, i.e., the stiffness ratio between the softening and loading paths for the normal bond, realistic values of UCS/UTS in the range of 10-30 (Hoek & Bieniawski 1965, Hoek & Martin 2014) can be achieved. The question we ask here is that given a particle assembly with a realistic UCS/UTS value, how do the failure behaviors transition from uniaxial tension to triaxial compression?

A better understanding of the strength behaviors in the mixed stress state is critical not only for modeling problems involving multiple failure modes, but also for rock mechanics testing. For example, validity of the Brazilian tensile test rests upon the premise of a tension cut-off as we are basically using the tensile strength under confinement as an indirect measure of the uniaxial tensile strength.

2 MODEL SETUP

Confined tension and compression tests are conducted with *PFC 5* (Itasca 2014a, b) using a rectangular particle assembly of 60 mm in width and 120 mm in height in 2D and a cylindrical sample of 40 mm in diameter and 80 mm in height in 3D. Particles of a uniform size distribution of radii $\bar{R} = 0.8 - 1.66$ mm are generated randomly within the simulation domain. The basic contact parameters for our user implemented displacement-softening contact model are listed in Table 1. The normal bond strength is set to be $\bar{\sigma}_c = 15 \pm 1.5$ MPa, and the shear bond strength is chosen to be $\bar{\tau}_c = 20\bar{\sigma}_c$ so that bond failure only occurs in the normal direction. For a softening coefficient $\beta = 0.1$, the corresponding macro-scale properties obtained from uniaxial compression and direct tension tests are given in Table 2. The strength ratio, UCS/UTS = 14.7, compares well with those of realistic rocks such as Berea sandstone.

Table 1. Basic contact parameters.

Point contact		Area contact (bond)	
point contact modulus	$E_c = 50$ GPa	parallel bond modulus	$\bar{E}_c = 50$ GPa
stiffness ratio	$\kappa = k_n/k_s = 4.0$	bond stiffness ratio	$\bar{\kappa} = \bar{k}_n/\bar{k}_s = 4.0$
friction coefficient	$\mu = 0.5$	contact radius multiplier	$\bar{\lambda} = 1$

Table 2. Macro-scale properties of the particle assembly.

	2D	3D
Young's modulus, Poisson's ratio	$E = 51.18$ GPa, $\nu = 0.29$	$\bar{E}_c = 50$ GPa, $\nu = 0.35$
uniaxial compressive strength	$\sigma_c = 93.53$ MPa	$\sigma_c = 111.02$ MPa
uniaxial tensile strength	$\sigma_t = 8.37$ MPa	$\sigma_t = 7.53$ MPa

3 RESULTS AND DISCUSSION

The numerical tests are conducted by first compressing the particle assembly isotropically and then either decreasing or further increasing the axial load with the horizontal confinement held constant. Stress states at failure are shown in Figure 1 for both the 2D and 3D simulations. Overall, Hoek-Brown criteria for intact rock fit the two sets of data very well. However, upon closer examination, the 2D Hoek-Brown envelope underestimates the uniaxial tensile strength, while the 3D envelope overestimates it (see Fig. 1(c)).

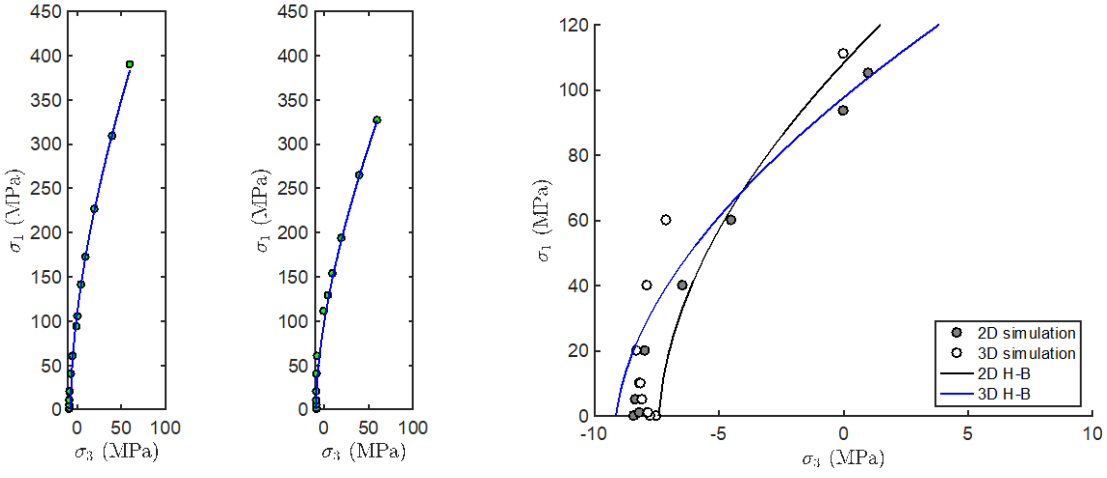

(a) (b) (c)

Figure 1. Stress states at failure from 2D (a) and 3D (b) simulations, fitted by Hoek-Brown criteria; a close up view (c); Hoek-Brown fitting parameters: $m = 14.47$, $\sigma_c = 108.28$ MPa for 2D and $m = 10.56$, $\sigma_c = 97.68$ MPa for 3D.

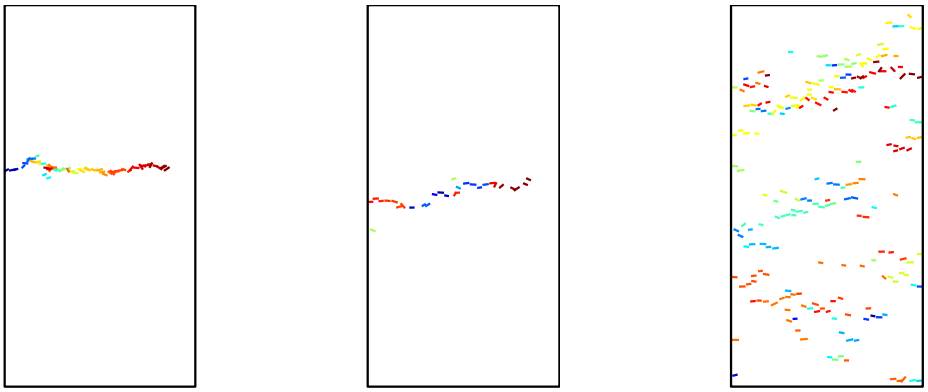

(a) (b) (c)

Figure 2. Accumulation of the micro-cracks at 90% post-peak from the 2D confined tension tests; (a) $\sigma_x = 0$, $\sigma_y = -8.37$ MPa, (b) $\sigma_x = 10$ MPa, $\sigma_y = -8.20$ MPa, (c) $\sigma_x = 60$ MPa, $\sigma_y = -4.51$ MPa; σ_x and σ_y are the horizontal and vertical stresses; compression positive; color marks the relative time when a micro-crack is formed following the jet colormap, blue for early time and dark brown for late time.

It is rather remarkable that the numerical results in fact share similarities with those observed from laboratory experiments (Brace 1960, Ramsey & Chester 2004, Bobich 2005) in that the tensile strength remains nearly constant if the magnitude of the confining stress is limited to a few times of the uniaxial tensile strength. In other words, our DEM simulations also support the existence of a tension cut-off. The mean tensile strength is $\bar{\sigma}_t = 8.24$ MPa for $\sigma_1 \lesssim 20$ MPa in 2D and $\bar{\sigma}_t = 7.85$ MPa for $\sigma_1 \lesssim 60$ MPa in 3D.

Denote ω as the ratio of the limiting confining stress where the tension cut-off ends over the uniaxial tensile strength. For the 2D simulations, $\omega \approx 2.4$ is comparable to the threshold of $\omega = 3$ from the original Griffith's criterion. For the 3D simulations, $\omega \approx 7.6$ is very close to the value observed in Ramsey and Chester (2004) and also the prediction of $\omega = 7.8$ by Fairhurst (1964), where $\omega = w(w-2)$ and $w = \sqrt{\sigma_c/\sigma_t}$. As far as the 3D extension of Griffith's criterion by Murrell (1963) is concerned, the tension cut-off terminates at $\omega = 5$ for $\sigma_1 > \sigma_2 = \sigma_3 = -\sigma_t$ and $\omega = 21.39$ for $\sigma_1 = \sigma_2 > \sigma_3 = -\sigma_t$. This means Murrell's criterion overestimates the value of ω for the triaxial extension state when compared with our simulations.

For the triaxial extension tests, as the confining stress increases, the macro-scale failure mechanisms evolve from a well-defined mode I tensile crack, a tensile crack with tortuous step-like features, to multiple tensile crack bands, which resemble the shear bands in the compression tests (see Fig. 2). At the micro-scale, majority of the micro-cracks are aligned in the direction of the major principal stress. Inclinations of the stepped portion in Figure 2(b) and the crack bands in Figure 2(c) are roughly 20° with respect to the horizontal direction.

Unfortunately, the particular stress path we chose does not yield meaningful simulation results when the confinement in the extension test is above 60 MPa. Bond breakage has already occurred when the sample is compressed isotropically beyond 60 MPa. Further study with different stress paths and true triaxial stress state will therefore be needed to provide more insights.

4 CONCLUSIONS

A fundamental rock mechanics question regarding the intact rock strength behaviors under confined tension is investigated numerically using *PFC 5* with a user implemented displacement-softening model. Our analysis gives the first numerical evidence that supports the use of a tension cut-off in failure criteria. The numerical results regarding the limiting confining stress for the tension cut-off and the transition of failure behaviors from a mode I tensile crack to inclined crack bands are consistent with laboratory observations in the literature.

REFERENCES

Bobich, J.K. 2005. *Experimental Analysis of the Extension to Shear Fracture Transition in Berea Sandstone*. Master's thesis, Texas A&M University.

Brace, W.F. 1964. State of stress in the earth's crust. In W. R. Judd (ed), *Brittle Fracture of Rocks*: 110–178. Elsevier, New York.

Fairhurst, C. 1964. On the validity of the Brazilian test for brittle materials. *Int. J. Rock Mech. Min. Sci.*, 1(4):535–546.

Hoek, E. & Bieniawski, Z. T. 1965. Brittle fracture propagation in rock under compression. *Int. J. Fract. Mech.*, 1(3):137–155.

Hoek, E. & Martin, C. D. 2014. Fracture initiation and propagation in intact rock–a review. *J. Rock Mech. Geotech. Engng.*, 6(4):287–300.

Huang, H. 1999. *Discrete Element Modeling of Tool-Rock Interaction*. PhD thesis, University of Minnesota.

Itasca Consulting Group, Inc. 2014a. *PFC2D – Particle Flow Code in 2-Dimensions, Ver. 5.0*. Minneapolis: Itasca.

Itasca Consulting Group, Inc. 2014b. *PFC3D – Particle Flow Code in 3-Dimensions, Ver. 5.0*. Minneapolis: Itasca.

Ma, Y. & Huang, H. 2018. A displacement-softening contact model for discrete element modeling of quasi-brittle materials. *Int. J. Rock Mech. Min. Sci.*, 104, 9-19.

Murrell, S.A.F. 1963. A criterion for brittle fracture of rocks and concrete under triaxial stress and the effect of pore pressure on the criterion. In C. Fairhurst (ed.), *Rock mechanics* (*Proc. 5th Symp. on Rock Mechanics)*: 563-577 Pergamon Press, Oxford.

Potyondy, D.O. & Cundall, P.A. 2004. A bonded-particle model for rock. *Int. J. Rock Mech. Min. Sci.*, 41(8):1329–1364.

Ramsey, J.M. & Chester, F.M. 2004. Hybrid fracture and the transition from extension fracture to shear fracture. *Nature*, 428(6978):63–66.